

^3He Impurities on the Bulk Surface of Liquid ^4He : Possible Existence of Excited States

Nicolas Pavloff and Jacques Treiner

Division de Physique Théorique, Institut de Physique Nucléaire, Orsay, France*

(Received September 26, 1990)

We study, using a density-functional approach, the properties of the two-dimensional system formed by ^3He atoms on the surface of liquid ^4He , as a function of ^3He coverage N_s , at zero temperature. We find several types of surface states accessible to the ^3He atoms. For small values of N_s , the surface tension σ is, as expected, linear in N_s^2 . For a coverage of about half a monolayer, a new type of surface state starts being occupied, and this produces a change in the slope of σ as a function of N_s^2 and, more clearly, a step in the surface specific heat, which increases by a factor of almost two. Another step is predicted to occur for a coverage of ~ 1.3 monolayer. Existing data are compatible with this structure of surface states but are not numerous enough to prove or disprove the existence of steps.

1. INTRODUCTION

The surface tension σ of liquid ^4He at low temperatures depends strongly on the presence of small ^3He impurities. For ^3He concentrations less than one atomic layer, σ decreases by almost 25%, compared to its value for pure ^4He . This fact was correctly interpreted a long time ago by Andreev¹ as the signature of the existence of surface states with larger binding energy than that of a ^3He atom in the bulk of liquid ^4He . When the temperature is sufficiently low, the ripplon contribution to the surface tension becomes negligible, and $\sigma(T)$ exhibits the typical T^2 -dependence of a two-dimensional Fermi gas (2-DFG). This system has been studied experimentally by several groups for various ^3He coverages.²⁻⁶ In addition to the surface tension, Edwards *et al.*^{4,5} have also measured the velocity of "surface second sound," a compression mode of the two-dimensional Fermi gas predicted by Andreev and Kompaneets.⁷

* Unité de Recherche des Universités Paris 11 et Paris 6 Associée au CNRS.

The whole set of experimental data has been analyzed by Edwards *et al.*^{4,5} using an extension of the original Andreev model to the case of (weakly) interacting particles. The quasiparticle energy spectrum is expressed as

$$\varepsilon(k) = \varepsilon_0 + \frac{\hbar^2}{2M_0} k^2 + \frac{1}{2} N_s V_0^s \quad (1)$$

where ε_0 denotes the energy of the Andreev ground state with respect to a free ${}^3\text{He}$ atom in the limit of infinite dilution, M_0 its (surface) effective mass, and k a momentum parallel to the surface which has a maximum value k_f , related to the number of ${}^3\text{He}$ atoms per unit surface N_s by

$$N_s = \frac{k_f^2}{2\pi} \quad (2)$$

The quantity V_0^s characterizes the strength of the interaction between the surface ${}^3\text{He}$ atoms. Expressions involving the three quantities ε_0 , M_0 , and V_0^s can be derived for the surface tension and the velocity of surface sound. In Ref. 4 the values resulting from the fit to the data was found to be (m_3 denotes the bare mass of a ${}^3\text{He}$ atom)

$$\varepsilon_0 = (-5.08 \pm 0.03) \text{ K}$$

$$\frac{M_0}{m_3} = 1.3 \pm 0.1$$

$$V_0^s = (0.5 \pm 2) 10^{-31} \text{ erg cm}^2 \\ = (3.6 \pm 14.5) \text{ K \AA}^2$$

whereas in Ref. 5, inclusion of data for smaller and larger ${}^3\text{He}$ coverage lead to

$$\varepsilon_0 = (-5.02 \pm 0.03) \text{ K}$$

$$\frac{M_0}{m_3} = 1.45 \pm 0.1$$

$$V_0^s = (11.6 \pm 10.1) \text{ K \AA}^2$$

The theoretical studies of this system have been often devoted to the limiting case of *one* ${}^3\text{He}$ atom on the surface of liquid ${}^4\text{He}$. Of course in this limit one does not have to consider a quasiparticle interaction. The most popular approach is the Lekner-Feynman theory (see Refs. 8-12), where the properties of the system are described by the solution of a Schrödinger equation in which only the asymptotic behaviors of the effective

potential experienced by the ^3He atom are well determined (they are related to the properties of pure ^4He). They provide a semiquantitative understanding of the surface states, except for the existence of an effective mass larger than the bare mass.

In Ref. 13, Dalfovo and Stringari have addressed this question using a density functional method, already proposed for the description of pure ^3He and ^4He as well as for homogeneous mixtures of the two isotopes. Extension to spherical clusters has been discussed by Dalfovo.¹⁴ They found values close to those quoted above ($\varepsilon_0 = -5.4$ K and $M_0/m_3 = 1.3$) and the interesting result that there was an excited state (one node in the wavefunction) with energy $\varepsilon_1 = -3.6$ K and effective mass $M_1/m_3 = 1.7$. It was also shown that the existence of this excited state was closely related to the shape of the density profile of pure ^4He ; the larger its surface thickness, the smaller the localization and the kinetic energy of the ^3He atom—hence, more binding. The surface thickness of pure ^4He was found to be 7 \AA in Ref. 15, in agreement with the microscopic calculations of large clusters of Ref. 16. This value is significantly larger than that used in the previous calculations of ε_0 , where only one bound state was obtained.

A more elaborate density functional has recently been proposed,¹⁷ using a finite range interaction and incorporating hard-core effects, both features absent in Refs. 13–15. For homogeneous systems, however, it is identical to the functional used in Ref. 13. When generalized to helium mixtures and applied to the study of ^3He impurity states on the bulk surface,¹⁸ one obtains the same structure of states as in Ref. 13, with values for the energies and the effective masses: (-5.20 K, $1.35m_3$) and (-3.16 K, $1.74m_3$), respectively; these differences with respect to Ref. 13 are due to the slightly smaller surface thickness obtained in Ref. 17 compared to Ref. 15, namely 5.8 \AA , but the general physical picture remains the same.

At this point, one might object that the ^4He surface profile of $\approx 4 \text{ \AA}$ used by Sherrill and Edwards¹² or more recently by Anderson and Miller¹⁹ to study the ^3He impurity states was deduced from a study of the scattering of ^4He atoms by the free surface.⁵ However, it was clearly stated in Ref. 20 that the scattering of ^4He atoms was essentially determined by the asymptotic behavior of the *average field*, which does not put strong constraints on the width of the *density profile*. Indeed, one can show that the model of Ref. 17, when applied to the scattering problem, gives results in excellent agreement with experiment.²¹ Hence we feel that it is worth considering the possible consequences of a larger ^4He surface thickness.

The purpose of the present work is to investigate in a self-consistent framework the dependence on the ^3He coverage of the various quantities characterizing the system (energies, effective masses, density profiles, average fields, surface tension, and surface specific heat) and to determine

a possible experimental signature of the existence of several types of Andreev states. We will use the functional of Ref. 13. As the fermions are treated in a mean-field approximation, it has the advantage of leading to differential equations rather than integro-differential equations rather than integro-differential equations, which would be the case with the method of Ref. 18.

Notice that the states we are interested in are different from those investigated by Krotscheck and coworkers^{22,23} in thin mixture films. In these systems, the strong potential of the substrate plays an essential role in determining the impurity potential and modifies substantially the properties of the surface states. A study of the variation of the structure of ^3He states with film thickness, in the limiting case of one ^3He atom, is presented in Ref. 18, where it is shown that the *asymptotic* surface impurity potential is obtained only for ^4He coverage larger than $\sim 0.6 \text{ \AA}^{-2}$, i.e., eight atomic layers, whereas coverages smaller than 0.3 atomic layers were considered in Refs. 22 and 23. Let us indicate here that the mean-field approach used in the present work is unable to produce the layered structure of thin films on a substrate. As mentioned above, the effective interaction from which the density functional is constructed misses the characteristic distance of the repulsive hard core, and its Fourier transform, diverging for large momenta, prevents the system from developing large oscillations of the density, even in a strong external field. This deficiency would be less important in the description of the surface of thick films and has a minor effect for the bulk surface, so we expect the method to be as accurate here as it was in the description of helium clusters²⁴ or the free surface of both isotopes.¹⁵ The ability of the present density functional to describe correctly the system was established by Dalfovo in Ref. 14 by a careful comparison with the Lekner-Feynman theory, in the case of ^3He impurities on ^4He droplets.

The paper is organized as follows. The energy density functional is presented in Sec. 2.1. The coupled equations to be solved self-consistently are derived in Sec. 2.2. For small coverage, one can use perturbation theory to analyze how the presence of the interactions between the helium atoms affects the ideal behavior of the two-dimensional Fermi gas. This is done in Sec. 2.3, where we also discuss the connection between the present model and that of Edwards *et al.*⁴ The numerical procedure is described in Sec. 2.4. Our results are presented in Sec. 3: evolution of the ^4He profile and of the mean-field experienced by the surface ^3He atoms (3.1), ^3He single-particle spectrum and wavefunctions (3.2), surface tension (3.3), and effective masses (3.4). When the second continuum starts being occupied, the density of states near the Fermi energy increases abruptly, and we analyze in Sec. 3.5 the resulting effect on the surface specific heat of the system. In Sec. 4, a comparison is made with unpublished data by Edwards and coworkers and

with the heat capacity measurements on *thick* films by Gasparini and coworkers. Finally our conclusion are presented in Sec. 5.

2. A MEAN-FIELD APPROXIMATION

2.1. The Energy Density Functional

The functional has already been introduced in Refs. 13, 14, and 25, and we refer the reader to these papers and to Ref. 26 for a detailed discussion of its structure. An effective interaction of Skyrme type²⁷ is used in a mean-field approximation in which the ground-state wavefunction is antisymmetric with respect to the exchange of two ${}^3\text{He}$ atoms and symmetric with respect to the exchange of two ${}^4\text{He}$ atoms. The resulting expression of the energy of an inhomogeneous mixture of liquid ${}^3\text{He}$ and ${}^4\text{He}$ at zero temperature appears as a functional of the number densities ρ_3 and ρ_4 and the kinetic energy densities τ_3 and τ_4

$$\rho_3(\mathbf{r}) = 2 \sum_i \int d^2k |\phi_3^{i,k}(\mathbf{r})|^2 \quad (3)$$

$$\tau_3(\mathbf{r}) = 2 \sum_i \int d^2k |\nabla \phi_3^{i,k}(\mathbf{r})|^2 \quad (4)$$

$$\tau_4(\mathbf{r}) = \frac{1}{4} \frac{|\nabla \rho_4(\mathbf{r})|^2}{\rho_4(\mathbf{r})} \quad (5)$$

where \mathbf{k} denotes a momentum parallel to the surface.

In Eqs. (3) and (4), the sum over the occupied states of ${}^3\text{He}$ contains a discrete part corresponding to the different types of bound states and an integral over the momentum parallel to the surface. Each type of bound states constitutes a two-dimensional continuum labeled by an index i , to which corresponds a two-dimensional Fermi momentum k_{fi} .

In the case of pure ${}^3\text{He}$ or pure ${}^4\text{He}$, the functional reduces to the form used in Refs. 15 and 24. The parameters are fixed by the experimental values of the equilibrium density, the energy per particle, the compressibility, and the surface tension of each system. In the case of homogeneous mixtures with small concentrations of ${}^3\text{He}$ atoms, it reduces to the functional proposed in Ref. 25.

The form of the functional is

$$E = \int d^3r \mathcal{H}(\mathbf{r}) \quad (6a)$$

$$\begin{aligned} \mathcal{H}(\mathbf{r}) = & \frac{\hbar^2}{2m_3^*} \tau_3 + \frac{\hbar^2}{2m_4} \tau_4 + U(\rho_3, \rho_4) + d_3 |\nabla \rho_3|^2 \\ & + d_4 |\nabla \rho_4|^2 + d_{34} \nabla \rho_3 \nabla \rho_4 \end{aligned} \quad (6b)$$

where $U(\rho_3, \rho_4)$ is an algebraic function of the densities ρ_3 and ρ_4 given explicitly in the appendix. The functional involves the gradients of the number densities. In absence of a finite-range interaction, these terms are essential for a correct description of the surface properties; they also give rise to an effective mass depending on the number densities ρ_3 and ρ_4 . This effective mass is parametrized in the form

$$\frac{\hbar^2}{2m_3^*(\mathbf{r})} = \frac{\hbar^2}{2m_3} \left(1 - \frac{\rho_3(\mathbf{r})}{\rho_{3c}} - \frac{\rho_4(\mathbf{r})}{\rho_{4c}} \right)^2 \quad (6c)$$

where ρ_{3c} and ρ_{4c} are constant; m_3 (resp. m_4) denotes the mass of a ${}^3\text{He}$ (resp. ${}^4\text{He}$) atom.

In view of the small difference existing between the ${}^3\text{He}$ - ${}^3\text{He}$ and the ${}^4\text{He}$ - ${}^4\text{He}$ effective interactions ($d_3 \simeq d_4$), the coefficient d_{34} , which characterizes the ${}^3\text{He}$ - ${}^4\text{He}$ interaction in the surface, was chosen in Ref. 14 as

$$d_{34} = d_3 + d_4 \quad (7)$$

where it was shown that the results did not depend much on its precise value.

The functional is finally characterized by 15 parameters, some being better determined than the others. Ten of them are directly related to the pressure-density relation and the surface tension of pure ${}^3\text{He}$ and ${}^4\text{He}$ and to the density dependence of the effective mass of a ${}^3\text{He}$ atom, which are well-known physical properties. Among the five remaining coefficients, four were fixed in Refs. 25 and 26 in order to reproduce several thermodynamic properties of homogeneous mixtures: excess volume parameter, ${}^3\text{He}$ chemical potential, excess of enthalpy, and osmotic pressure. We have checked that our results are stable against small changes in these coefficients. Only changes in d_{34} may quantitatively affect the present results (see below, Sec. 3.3). However, for sake of coherence, we have kept the values used in previous studies.

2.2. The Mean-Field Equations

The equilibrium configuration is obtained by minimizing the total energy of the system with respect to the function $\phi_4(\mathbf{r}) = \sqrt{\rho_4(\mathbf{r})}$ and to the wavefunctions $\phi_3^{i,k}(\mathbf{r})$, under the constraints of normalization of the $\phi_3^{i,k}(\mathbf{r})$'s and that ρ_4 should go asymptotically, i.e., away from the surface, to the equilibrium density of pure ${}^4\text{He}$. One thus introduced Lagrange

multipliers $\varepsilon_{i,k}$ (we do not write explicitly their dependence on N_s) and μ_4 , and minimizes the form

$$E - 2 \sum_i \int d^2k \varepsilon_{i,k} \int |\phi_3^{i,k}(\mathbf{r})|^2 d^3r - \mu_4 \int \rho_4(\mathbf{r}) d^3r \quad (8)$$

By considering the bulk liquid, one sees that μ_4 is just the chemical potential of pure liquid ⁴He. The resulting equations read as

$$-\nabla \frac{\hbar^2}{2m_3^*} \nabla \phi_3^{i,k} + V_3 \phi_3^{i,k} = \varepsilon_{i,k} \phi_3^{i,k} \quad (9a)$$

$$\frac{\hbar^2}{2m_4} \nabla^2 \phi_4 + V_4 \phi_4 = \mu_4 \phi_4 \quad (9b)$$

where the average field $V_3(\mathbf{r})$ (resp. $V_4(\mathbf{r})$) of the ³He (resp. ⁴He) atoms are given by

$$V_3(\mathbf{r}) = \frac{\partial U}{\partial \rho_3} - 2d_3 \nabla^2 \rho_3 - d_{34} \nabla^2 \rho_4 + \frac{\partial}{\partial \rho_3} \left(\frac{\hbar^2}{2m_3^*} \right) \tau_3 \quad (10a)$$

$$V_4(\mathbf{r}) = \frac{\partial U}{\partial \rho_4} - 2d_4 \nabla^2 \rho_4 - d_{34} \nabla^2 \rho_3 + \frac{\partial}{\partial \rho_4} \left(\frac{\hbar^2}{2m_3^*} \right) \tau_3 \quad (10b)$$

We can now make use of the geometry of the problem. The translational invariance parallel to the surface allows one to look for solutions of the form

$$\phi_3^{i,k}(\mathbf{r}) = \frac{1}{2\pi} \phi_3^{i,k}(z) e^{i(k_x x + k_y y)} \quad (11)$$

where we choose the z axis perpendicular to the surface. It follows from Eq. (3) that ρ_3 will depend on z only (the same will be true for ρ_4). Notice that

$$N_s = \int_{-\infty}^{+\infty} \rho_3(z) dz \quad (12)$$

and that Eqs. (3 and 4) take the form

$$\rho_3(z) = \sum_i \int_0^{k_{f_i}} \frac{k dk}{\pi} |\varphi_3^{i,k}(z)|^2 \quad (13)$$

$$\tau_3(z) = \sum_i \int_0^{k_{f_i}} \frac{k dk}{\pi} \left(\left| \frac{d\varphi_3^{i,k}(z)}{dz} \right|^2 + k^2 |\varphi_3^{i,k}(z)|^2 \right) \quad (14)$$

whereas Eq. (9a) can now be written as

$$\begin{aligned} & -\frac{\hbar^2}{2m_3^*(z)} \frac{d^2 \varphi_3^{i,k}(z)}{dz^2} - \frac{d}{dz} \left(\frac{\hbar^2}{2m_3^*(z)} \right) \frac{d\varphi_3^{i,k}(z)}{dz} + \left(V_3(z) + \frac{\hbar^2}{2m_3^*(z)} k^2 \right) \varphi_3^{i,k}(z) \\ & = \varepsilon_{i,k} \varphi_3^{i,k}(z) \end{aligned} \quad (15)$$

where $k^2 = k_x^2 + k_y^2$ is the magnitude of the momentum parallel to the surface. This equation shows that, as expected, $\varphi_3^{i,k}$ and $\varepsilon_{i,k}$ depends only on k . In this one-dimensional geometry, the Laplacian operators appearing in Eqs. (10a, b) can be replaced by second order derivatives. The equation for $\rho_4(z)$, derived from Eq. (9b) then reads as

$$\frac{\hbar^2}{2m_4} \frac{1}{4} \left(\frac{\rho_4'^2}{\rho_4^2} - 2 \frac{\rho_4''}{\rho_4} \right) + V_4 = \mu_4 \quad (16)$$

Once one has solved Eqs. (15) and (16), one can compute the surface tension of the system as

$$\sigma = \int_{-\infty}^{+\infty} \mathcal{H}(z) dz - \mu_3 N_s - \mu_4 \int_{-\infty}^{+\infty} \rho_4(z) dz \quad (17)$$

where μ_3 denotes the chemical potential of the ^3He atoms. If different types of surface states are occupied, to each type of states correspond a continuum in energy $\varepsilon_{i,k}$ and one has of course

$$\mu_3 = \varepsilon_{i,k_f i} \quad \text{for all occupied } i \text{ state} \quad (18)$$

2.3. Connection with the Model of Edwards *et al*⁴

For small coverage, we only have to consider one continuum, namely that built on the ground state $\varphi_3^{0,0}$ (no node in the wavefunction). The term in k^2 in Eq. (15) is small compared to the average field $V_3(z)$, so that first-order perturbation theory gives, for a given k_f

$$\varepsilon_{0,k} \approx \varepsilon_{0,0} + \frac{\hbar^2}{2M_0} k^2 \quad (19a)$$

where

$$\frac{\hbar^2}{2M_0} = \int_{-\infty}^{+\infty} \varphi_3^{0,0} \frac{\hbar^2}{2m_3^*(z)} \varphi_3^{0,0} dz \quad (19b)$$

Equation (19a) is not in disagreement with Eq. (1) because the ground-state energy $\varepsilon_{0,0}$ (as well as $\varphi_3^{0,0}$) depends on N_s , as $V_3(z)$ and $m_3^*(z)$ do.

Concerning the structure of the surface tension for small ^3He coverage, one can proceed as follows. Let us evaluate the change $d\sigma$ in the surface tension when one increases the surface ^3He density by dN_s . We denote by $\delta\rho_3(z)$ (resp. $\delta\rho_4(z)$) the change in $\rho_3(z)$ (resp. $\rho_4(z)$). Upon expanding σ in powers of dN_s , one obtains, to first order

$$d\sigma \approx \int \frac{\delta\mathcal{H}}{\delta\rho_3} \delta\rho_3 dz + \int \frac{\delta\mathcal{H}}{\delta\rho_4} \delta\rho_4 dz - d\mu_3 N_s - \mu_3 dN_s - \mu_4 \int \delta\rho_4(z) dz \quad (20)$$

where the variations of \mathcal{H} are functional variations, equal, from Eqs. (15) and (16), to μ_3 and μ_4 respectively. One is then left with

$$d\sigma \approx -N_s d\mu_3 \quad (21)$$

which proves that σ starts, for small N_s , as a quadratic function of N_s . We show in the appendix that, in the same limit, σ can be written as

$$\sigma \approx \sigma_4 - \frac{\pi \hbar^2}{2M_0} N_s^2 - (\Sigma_{33} + \Sigma_{34} + \Sigma_{44}) N_s^2 \quad (22a)$$

where the terms Σ_{33} , Σ_{34} , and Σ_{44} are generated respectively by the ³He-³He, ³He-⁴He, and ⁴He-⁴He interactions. When the second continuum is occupied, Eq. (22a) generalizes to

$$\sigma \approx \sigma_4 - \frac{\pi \hbar^2}{2M_0} \left(\frac{k_{f_0}^2}{2\pi} \right)^2 - \frac{\pi \hbar^2}{2M_1} \left(\frac{k_{f_1}^2}{2\pi} \right)^2 - (\Sigma_{33} + \Sigma_{34} + \Sigma_{44}) N_s^2 \quad (22b)$$

Formula (22a) is similar to the zero-temperature expression of Ref. 4 for the surface tension (see the discussion in the appendix). Here, however, we work with a more detailed model and through self-consistency we have an insight on the modification of the ⁴He profile as more ³He atoms are added to the surface as well as on the development of the ³He mean field (see Sec. 3).

2.4. The Numerical Procedure

The set of Eqs. (15) and (16) are solved by iteration, using the Numerov method, after linearization in the form

$$\frac{d^2 \varphi_3^{i,k}}{dz^2} = W_3 \varphi_3^{i,k} \quad (23a)$$

$$\frac{d^2 \rho_4}{dz^2} = W_4 \rho_4 \quad (23b)$$

The functions W_3 and W_4 are calculated with the solutions $\varphi_3^{i,k}$ and ρ_4 obtained at step n ; solving Eqs. (23a, b) provides $\varphi_3^{i,k}$ and ρ_4 at step $n+1$. One starts the calculations with a small ³He coverage, for which the initial guess for $\varphi_3^{i,k}$ is the ground-state wavefunction corresponding to $k_f = 0$, and for ρ_4 , the density profile of pure ⁴He. The solutions obtained after convergence for a given k_f are used as initial guesses for the next value of k_f . We have used a step in k_f of 0.05 \AA^{-1} .

Two types of integrals over k have to be performed (see Eqs. (13) and (14)), with weight k and k^3 . We have checked that a four-point Gaussian integration formula (see Ref. 28) provides an excellent accuracy. For each

value of k_{f_i} , Eqs. (15) and (16) have thus to be solved for 10 different values of k , including the value $k = 0$ and the value of the Fermi momentum $k = k_{f_i}$.

We shall now derive a relation that we use to test the convergence of the numerical solutions of the set of Eqs. (15) and (16). We multiply Eq. (15) by $d\varphi_3^{i,k}/dz$, Eq. (16) by $d\rho_4/dz$, add them together and integrate from $-\infty$ to z (we choose to put the bulk liquid in the direction $z < 0$). One then sums over i and k . The following result is obtained

$$\begin{aligned} & \frac{\hbar^2}{2m_3^*} \sum_i \int_0^{k_{f_i}} \frac{k dk}{\pi} \left[- \left| \frac{d\varphi_3^{i,k}}{dz} \right|^2 + k^2 |\varphi_3^{i,k}|^2 \right] - \frac{\hbar^2}{2m_4} \frac{1}{4} \frac{\rho_4'^2}{\rho_4} + U(\rho_3, \rho_4) \\ & - d_3 \rho_3'^2 - d_4 \rho_4'^2 - d_{34} \rho_3' \rho_4' = \sum_i \int_0^{k_{f_i}} \frac{k dk}{\pi} \varepsilon_{i,k} |\varphi_3^{i,k}|^2 + \mu_4 \rho_4 \end{aligned} \quad (24)$$

This relation implies that the sum of the derivative terms appearing in the integrand of Eq. (8) are equal to the sum of the bulk terms. We now integrate Eq. (24) over z and define two quantities I_v and I_s by

$$\begin{aligned} I_v = \int_{-\infty}^{+\infty} dz \left[\frac{\hbar^2}{2m_3^*} \sum_i \int_0^{k_{f_i}} \frac{k dk}{\pi} k^2 |\varphi_3^{i,k}|^2 + U(\rho_3, \rho_4) - \mu_4 \rho_4 \right] \\ - \sum_i \int_0^{k_{f_i}} \frac{k dk}{\pi} \varepsilon_{i,k} \end{aligned} \quad (25a)$$

$$\begin{aligned} I_s = \int_{-\infty}^{+\infty} dz \left[\frac{\hbar^2}{2m_3^*} \sum_i \int_0^{k_{f_i}} \frac{k dk}{\pi} \left| \frac{d\varphi_3^{i,k}}{dz} \right|^2 \right. \\ \left. + \frac{\hbar^2}{2m_4} \frac{1}{4} \frac{\rho_4'^2}{\rho_4} + d_3 \rho_3'^2 + d_4 \rho_4'^2 + d_{34} \rho_3' \rho_4' \right] \end{aligned} \quad (25b)$$

The equality of the two above expressions provides a strong test of the numerical accuracy of the calculation. The convergence is characterized by the quantity

$$\eta = \frac{I_v - I_s}{I_v + I_s} \quad (26)$$

For each value of N_s , one needs typically a hundred iterations in order to obtain a value of η of the order of 10^{-3} . The convergence is better for small values of N_s . We have also checked that, for all the values of N_s considered, the relevant quantities have converged and are stable.

3. RESULTS

3.1. Mean Field and Densities

The average field $V_3(z)$ experienced by the surface ${}^3\text{He}$ atoms is presented in Fig. 1, where we have also plotted the ${}^3\text{He}$ and ${}^4\text{He}$ density

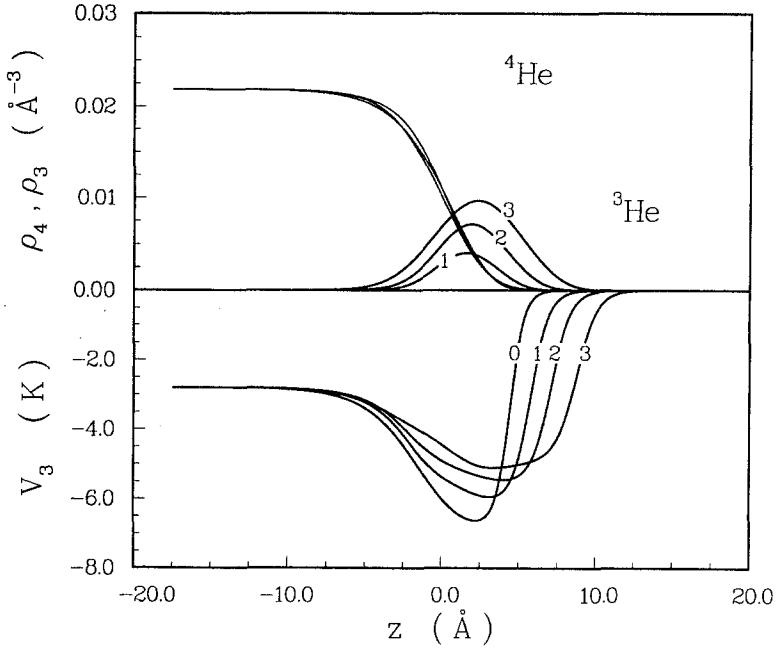


Fig. 1. ⁴He profile, ³He density, and mean-field experienced by the ³He atoms for various coverages. The labels 0, 1, 2, 3 refers respectively to $N_s = 0, 1.95 \times 10^{-2}, 3.98 \times 10^{-2},$ and $6.72 \times 10^{-2} \text{ \AA}^{-2}$. The ⁴He profile is drawn for cases 0, 2, and 3.

profiles. In the interior of the liquid $V_3(z)$ tends to the value of the chemical potential of a ³He atom in the bulk of liquid ⁴He, $V_3(-\infty) = -2.82 \text{ K}$. In the surface region $V_3(z)$ presents a well that admits different types of bound states (see below). One way of characterizing the width of the well is to consider the distance w between the two points z_1 and z_2 verifying

$$V_3(z_1) = V_3(z_2) = \frac{1}{2}(V_3(-\infty) + V_{3,\min}) \quad (27)$$

$V_{3,\min}$ being the minimum of the well. As N_s increases, w increases, starting from a minimum value of 6.25 \AA for $N_s = 0$. This value is significantly larger than the value found by Saam⁹ ($\sim 2 \text{ \AA}$) or Chang and Cohen¹¹ ($\sim 4 \text{ \AA}$), and this feature explains the existence of excited states not found in previous studies. The mean field $V_3(z)$ opens, as expected, on top of the liquid, and w reaches a value of $\sim 10 \text{ \AA}$ for a coverage of about one atomic layer.*

The ³He density profile follows the evolution of the mean field. As $V_3(z)$ opens, the maximum of $\rho_3(z)$ moves towards positive values of z . Through coupling and self-consistency, the density profile of the ⁴He atoms

* Following Edwards and Saam⁵ we define one atomic layer to have a number per unit area N_s equal to $(\rho_3^0)^{2/3} = 6.4 \times 10^{-2} \text{ \AA}^{-2}$, where ρ_3^0 is the number density in pure liquid ³He.

changes as more ${}^3\text{He}$ atoms are added to the system. Its surface thickness is defined as the distance between the points where the density has decreased by 10 and 90% with respect to the bulk value. At $N_s = 0$ it is equal to 7 \AA , then it decreases a minimum value (5.9 \AA) for $N_s \approx 0.035 \text{ \AA}^{-2}$. For larger N_s the surface thickness increases. This is in agreement with the finding of Dalfovo²⁶ that the width of the ${}^3\text{He}$ - ${}^4\text{He}$ interface (calculated with the same density functional as used here) is larger than the surface thickness of pure ${}^4\text{He}$.

3.2. Eigenstates

The single-particle energies $\varepsilon_{i,k}$ are plotted in Fig. 2. Actually what we plot are (i) the values of the energies $\varepsilon_{i,0}$ corresponding to $k = 0$ in Eq. (15) and (ii) the value of the Fermi energy μ_3 (see Eq. (18)). We find three types of states, the wavefunctions of which are shown in Fig. 3 (we only plot the wave functions corresponding to $k = 0$). A first series of states have no node in the wavefunction. The energy of the lowest of these states $\varepsilon_{0,0}$ increases linearly with N_s for $N_s \lesssim 0.035 \text{ \AA}^{-2}$. For $N_s \approx 0.035 \text{ \AA}^{-2}$, the Fermi energy reaches the value $\varepsilon_{1,0}$ of the lowest energy of the second type of states (one

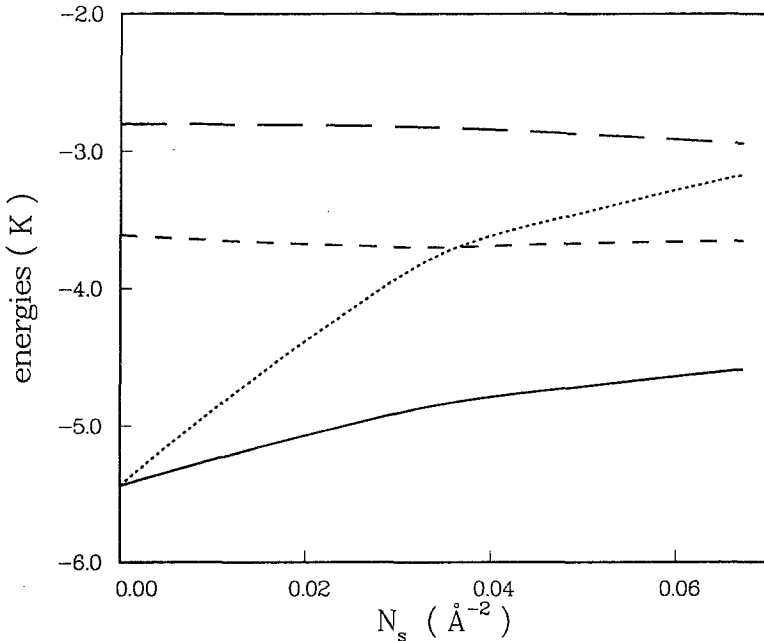


Fig. 2. Variation with N_s of the lowest energy of each type of surface states and of the Fermi energy. Continuous line: $\varepsilon_{0,0}$; dashed line: $\varepsilon_{1,0}$; dot-dashed line: $\varepsilon_{2,0}$; dotted line: μ_3 .

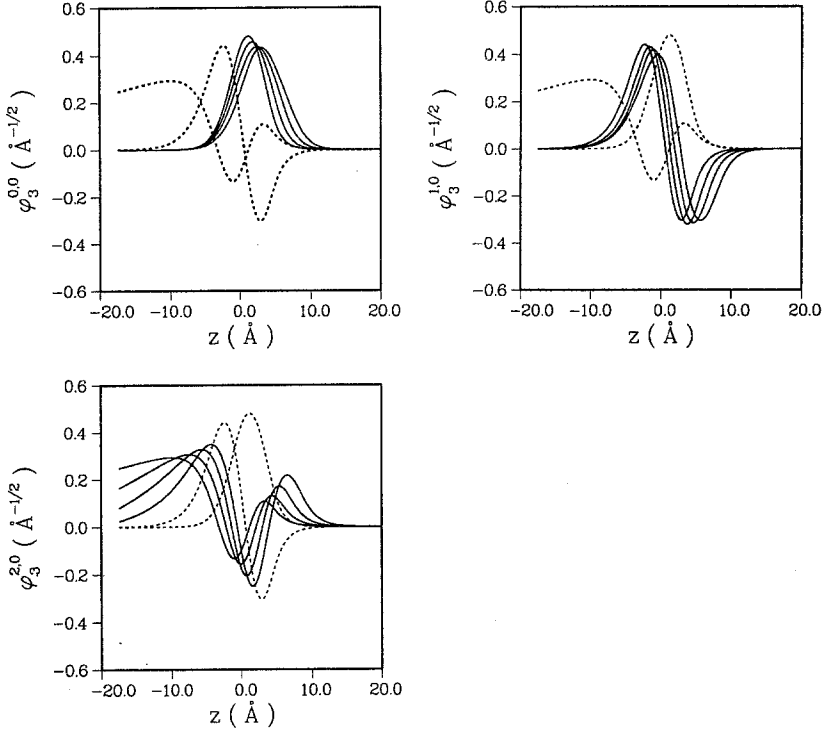


Fig. 3. Wavefunctions of the three Andreev states for various coverages. As in Fig. 1 the curves are drawn for the cases $N_s = 0, 1.95 \times 10^{-2}, 3.98 \times 10^{-2},$ and $6.72 \times 10^{-2} \text{\AA}^{-2}$. In each frame the dashed lines are the wave functions of the two other states for $N_s = 0$.

node in the wavefunction). The value of $\varepsilon_{1,0}$ appears not to depend on N_s . That it is so is linked to the evolution of the average field $V_3(z)$. As N_s increases, the minimum $V_{3,\min}$ becomes less negative, and the deepest state $\varepsilon_{0,0}$ is of course sensitive to this evolution. However the excited state $\varepsilon_{1,0}$ does not change because the well enlarges, and this enlarging happens to compensate a smaller depth.

This fact constitutes *the main result of the present work*: the excited state $\varepsilon_{1,0}$ found by Dalfovo and Stringari does survive when N_s increases, so that a second type of continuum states is available to the ³He atoms. For a ³He coverage larger than $\approx 0.035 \text{\AA}^{-2}$, i.e., half a monolayer, the density of states almost doubles. Consequently the variations of μ_3 with N_s is smaller. In this range, there are two Fermi momenta, one for each continuum, and one has of course

$$N_s = \frac{k_{f_0}^2}{2\pi} + \frac{k_{f_1}^2}{2\pi} = N_{s_0} + N_{s_1} \quad (28)$$

The third type of states (two nodes in the wavefunction, see Fig. 3) starts, for small coverage, with an energy close to that of an ^3He atom dissolved in the bulk. However, as more ^3He atoms are added to the surface, $\varepsilon_{2,0}$ decreases and reaches a value of ≈ -3 K when this state would start being occupied; from Fig. 2, this is expected to happen for $N_s \approx 0.08 \text{ \AA}^{-2}$, i.e., ~ 1.3 atomic layer.

3.3. Surface Tension

The values obtained by Edwards *et al.* in Ref. 5, quoted in the introduction, are represented as a shaded area in Fig. 4. As the authors did not indicate the largest coverage, the curves are drawn in the range of Ref. 4, i.e. $0 \leq N_s \leq 0.02 \text{ \AA}^{-2}$. As expected, the change in the surface tension $\Delta\sigma$ due to the ^3He impurities is a quadratic function of N_s and so are the numerical results (continuous line). The agreement between our calculated values and the values fitted to experiment is satisfactory, especially if one

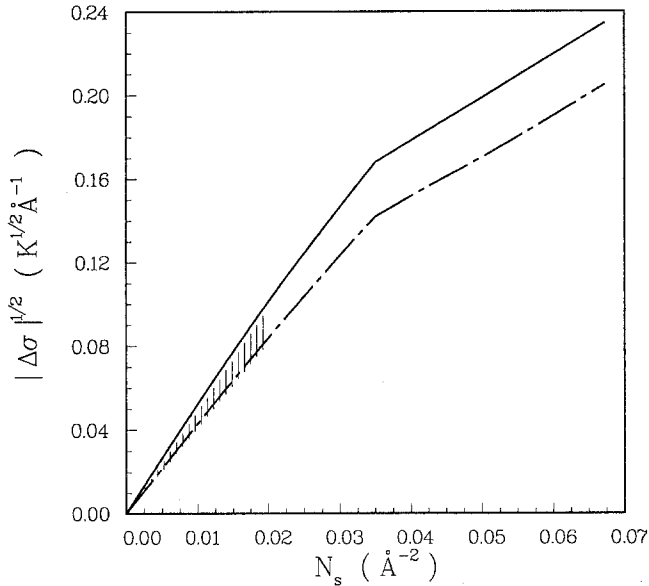


Fig. 4. Surface tension vs. ^3He coverage. The solid line represents the calculations of this paper. The dot-dashed line represents the Fermi gas contribution to the surface tension (ignoring the interaction term in Eq. (22a or b)). The results of the model of Edwards *et al.*⁴ lie (within experimental error) in the dashed area. The extremities of the dashed correspond to the case $V_0^s = 21.7 \text{ K \AA}^{-2}$, $M_0/m_3 = 1.35$ and $V_0^s = 1.5 \text{ K \AA}^{-2}$, $M_0/m_3 = 1.55$ which are the limits of experimental precision of Ref. 5. They stop at $N_s \approx 0.02 \text{ \AA}^{-2}$.

keeps in mind that the parameter d_{34} characterizing the ³He-⁴He interaction in the surface region was chosen according to Eq. (7) for sake of simplicity only and could be readjusted (a slightly larger value removes the remaining discrepancy).

In order to indicate the amplitude of the interaction terms to the surface tension, we have also plotted in Fig. 4 the simple Fermi gas result for $\Delta\sigma$. We see that the interaction represents 25–30% of the total value, and we find, in agreement with Edwards *et al.*,⁴ that it contributes to the decrease of σ (see the discussion in the appendix).

For ³He coverages such that the second continuum is occupied, a kink appears in $|\Delta\sigma|^{1/2}$; the change $\Delta\sigma$ becomes smaller than would be if the second type of states did not exist. This can be understood within the ideal 2-DFG model, where the surface tension, in the case of two types of states, can be written as

$$\sigma \approx \sigma_4 - \frac{\pi\hbar^2}{2M_0} \left(\frac{k_{f_0}^2}{2\pi} \right)^2 - \frac{\pi\hbar^2}{2M_1} \left(\frac{k_{f_1}^2}{2\pi} \right)^2 \quad (29)$$

where M_1 denotes the effective mass of a ³He in the second continuum, $M_1 \approx 1.6m_3$ (see below). Then, with the use of Eq. (28), one has

$$\sigma > \sigma_4 - \frac{\pi\hbar^2}{2M_0} \left[\left(\frac{k_{f_0}^2}{2\pi} \right)^2 + \left(\frac{k_{f_1}^2}{2\pi} \right)^2 \right] > \sigma_4 - \frac{\pi\hbar^2}{2M_0} N_s^2 \quad (30)$$

We conclude that the existence of a continuum of surface states with one node in the wavefunction should manifest itself in the dependence of σ as a function of ³He coverage. We shall now see, however, that a clearer signature is obtained by considering thermal properties which, as is well known, are governed by the effective mass.

3.4. Effective Masses

For each ³He coverage, we first check the validity of the two-dimensional Fermi gas model, implying that the single-particle energies are of the form (19a). We define a k -dependent effective mass through the relation

$$\varepsilon_{i,k} = \varepsilon_{i,0} + \frac{\hbar^2}{2m_{i,k}^*} k^2, \quad 0 \leq k \leq k_{f_i}, \quad i = 0, 1 \quad (31)$$

The ratio $m_{i,k}^*/m_{i,0}^*$ should not depend on k and be equal to 1 if the surface ³He atoms behaved as a Fermi gas. This is indeed the case, to a very good accuracy, for both types of surface states (for the largest coverage considered, one has $1 \leq m_{0,k}^*/m_{0,0}^* \leq 1.07$ and $1 \leq m_{1,k}^*/m_{1,0}^* \leq 1.01$). Hence, one can characterize the single-particle spectrum by two effective masses

M_0 and M_1 , independent of k , referring respectively to the first and second continuum. M_0 is calculated using Eq. (19b) and M_1 by a similar equation, namely

$$\frac{\hbar^2}{2M_1} = \int_{-\infty}^{+\infty} \varphi_3^{1,0}(z) \frac{\hbar^2}{2m_3(z)} \varphi_3^{1,0}(z) dz \quad (32)$$

Notice that M_0 and M_1 depend on N_s , so that the 2-DFG model is valid for a Fermi gas the characteristics of which are different for each ${}^3\text{He}$ coverage. The dependence of the effective masses on N_s are shown in Fig. 5. We note that in the range of ${}^3\text{He}$ coverages studied in Ref. 4, i.e., $0 \leq N_s \leq 0.02 \text{ \AA}^{-2}$, the calculated values of M_0/m_3 vary from 1.29 to 1.45. These values are to be compared to the ‘‘experimental’’ one quoted in the introduction. The quotation marks indicate here that the effective mass is not a primary quantity measured but a quantity derived through a model that did not consider its possible N_s dependence. We find that M_0 is almost a linear function of N_s , whereas M_1 stays constant up to $N_s \approx 0.02 \text{ \AA}^{-2}$ and then increases for larger values of the ${}^3\text{He}$ coverage. On the other hand, the effective mass of the second excited state is found to decrease from a value of $2.23m_3$ for $N_s = 0$ to $2m_3$ for one atomic layer. This is due to the constant decrease of the corresponding energy, indicating that this state becomes more localized in the surface region as N_s increases.

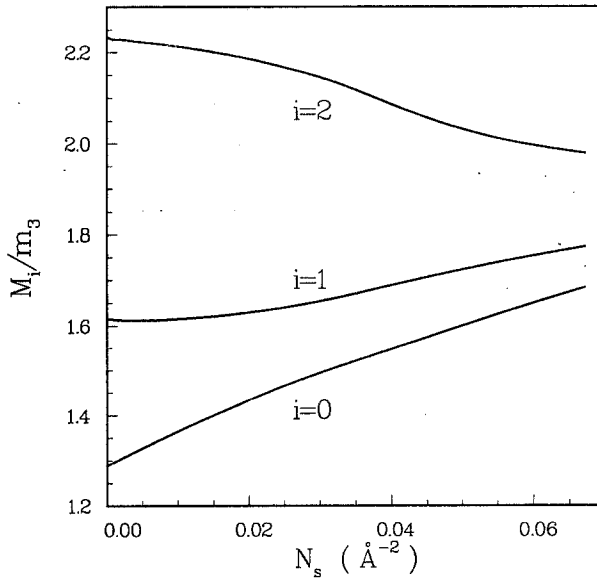


Fig. 5. Effective masses of the Andreev states (see Eqs. (19b) and (32)).

3.5. Specific Heat

At low temperature, the thermodynamic properties of an ideal two-dimensional Fermi gas are characterized by the level density parameter a , defined by

$$a = \frac{\pi^2}{6} g \quad (33)$$

where g is the single particle level density at the Fermi energy. Using Eq. (1), one finds, taking into account the spin degeneracy

$$g = \frac{k_f}{\pi} \left[\frac{d\varepsilon(k)}{dk} \right]_{k=k_f}^{-1} \approx \frac{M_0}{\pi \hbar^2} \quad (34)$$

In the case where the single-particle spectrum is not purely that of a Fermi gas, i.e., if one considers a possible slight k -dependence of the effective mass (see Sec. 3.4 above) then Eq. (34) is replaced by

$$g = \frac{m_{0,k_f}^*}{\pi \hbar^2} \left[1 - \frac{k_f}{2m_{0,k}^*} \frac{dm_{0,k}^*}{dk} \Big|_{k=k_f} \right]^{-1} \quad (35)$$

where $m_{0,k}^*$ is defined by Eq. (31). The correction brought by using Eq. (35) instead of Eq. (34) was found to be small: 3% for $N_s \approx 1$ atomic layer.

Equation (34) shows that for an ideal 2-DFG, g does not depend explicitly on the surface density. We have seen however in the preceding subsection that the effective masses did depend on N_s , so that the specific heat at constant volume per unit area

$$C_V = 2aT \quad (36)$$

shows a linear increase with N_s . This can be seen in Fig. 6 for $N_s \leq 0.035 \text{ \AA}^{-2}$. For $N_s \geq 0.035 \text{ \AA}^{-2}$, Eq. (34) must be generalized to the case of two continua. The single-particle level density is just the sum of the two single-particle level densities, so that one now has

$$g = g_0 + g_1 = \frac{M_0}{\pi \hbar^2} + \frac{M_1}{\pi \hbar^2} \quad (37)$$

The resulting curve is shown in Fig. 6 (in order to compare with experimental data, we plot C_V/T as a function of μ_3). Due to the almost doubling of the density of states when the second continuum starts being filled, there is a *discontinuity of the surface specific heat* of the system. The values of C_V/T jumps suddenly from 0.10 K^{-1} to 0.22 K^{-1} for $N_s \approx 0.035 \text{ \AA}^{-2}$. Although we have not calculated systems with $N_s > 0.067 \text{ \AA}^{-2}$,

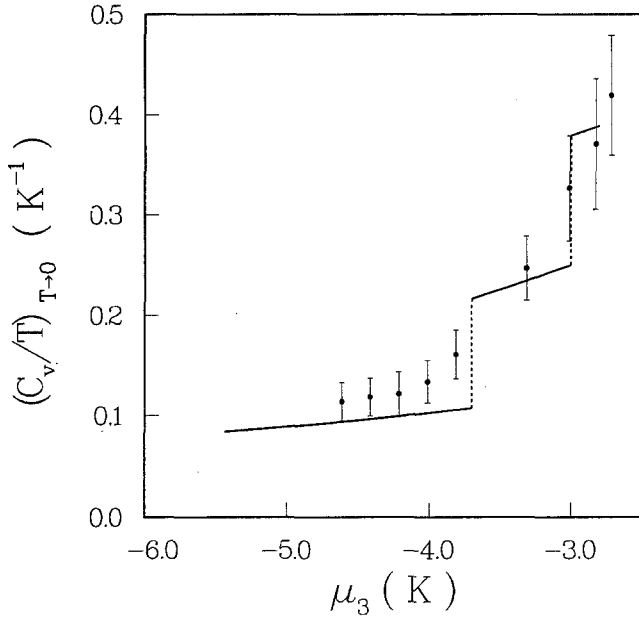


Fig. 6. Surface specific heat divided by temperature (extrapolated to zero temperature) as a function of the ^3He chemical potential. The position of the discontinuities in C_v/T are indicated by the vertical dotted lines. The experimental points and the error bars are taken from Ref. 31.

we indicate in Fig. 6 the effect expected from the occupation of the second type of excited states. The value of the effective mass M_2/m_3 was taken to be 1.98, obtained for the lowest of these states for $N_s = 0.067 \text{ \AA}^{-2}$.

Let us conclude this section by a brief comparison of our results with the work of Guyer, McCall, and Sprague.²⁹ This study was motivated by the observation of steps in the magnetization of thin mixture films.³⁰ However, neither the substrate potential nor the ^3He - ^4He interaction are included in the model, which is meant essentially to describe the development of a *self-bound* ^3He film. This is justified when the ^3He film is thick enough so that the presence of liquid ^4He becomes negligible. It is clearly not valid for small ^3He coverage, where the ^3He impurity acts like a probe of the ^4He profile. A connection between the model of Guyer *et al.*, and the present work can be made by considering the evolution of the energies of the impurity states. From our Fig. 2, it appears that only the second excited state has an energy decreasing with increasing ^3He coverage, as predicted in Ref. 30. Thus both models connect for coverage such that the

2D continuum built on this second excited state is being filled, i.e., for $N_s > 1.3$ atomic layer. It follows that the first step in C_V/T (or in the magnetization) is not due to the mechanism described in Ref. 30 but reflects directly properties of the ${}^4\text{He}$ ground state, in agreement with a Leckner understanding of the problem.

Another question related to the model of Ref. 29 is the maximum coverage N_s^{max} that the surface can support, at $T=0$, before ${}^3\text{He}$ atoms dissolve into the bulk. With one surface state with energy -5 K and effective mass $1.45m_3$, N_s^{max} is of the order of one atomic layer.⁵ In Ref. 29, by construction, there is no limitation to this quantity. In the present work, from Fig. 2, one extrapolates that the Fermi energy will reach the value -2.80 K before a new state appears in the potential well. Hence N_s^{max} is of the order of 1.5–2 atomic layers, larger than the value quoted in Ref. 5 but still finite. It is only after saturation of the bulk states (with 6% of ${}^3\text{He}$ atoms) that the film on top of the liquid would develop again, following the scheme of Guyer *et al.*

4. COMPARISON WITH EXPERIMENT FOR ${}^3\text{He}$ COVERAGE LARGER THAN 0.02 \AA^{-2}

As mentioned in the introduction, the most accurate set of data⁴ concerns simultaneous measurements of surface tension and surface second sound, for coverage smaller than 0.02 \AA^{-2} . We have already seen that our model gives a fairly good agreement with these data, which should be considered a prerequisite for any prediction concerning larger coverage. Less data are available in the domain of coverage where steps are predicted to occur in the surface specific heat, but we shall now see that the physical picture developed in the present work allows one to reinterpret existing data in a sense which confirms its validity.

The experimental points included in Fig. 6 are unpublished measurements by Crum, Edwards, and Sarwinski, taken from the Ph.D. thesis of Crum.³¹ The points are obtained from the surface entropy S divided by the temperature T , extrapolated to zero temperature; this quantity is identical to C_V/T , and an overall agreement in the general trend is obtained between theory and experiment (we have taken the energy of a ${}^3\text{He}$ atom in the bulk as a common reference for the theoretical and experimental values). The comment accompanying the figure in Ref. 31 was: "The fact that S/T is not constant for large μ_3 indicates that the two-dimensional gas model is not valid for large surface densities." Our results suggest an alternative interpretation, which explains the *rise* of C_V/T for μ_3 larger than -4 K: Indeed, the data are consistent with the existence of a simple Fermi gas up to $\mu_3 \approx -4$ K (the small slope of the curve is due to the dependence of the

effective mass on the ^3He coverage N_s); for larger values of N_s , the data are consistent with the superposition of two, then three Fermi gases built on the different types of surface states. Notice that the experimental points are not numerous enough, in the range of coverage where we predict the occurrence of steps in C_V/T , either to confirm or disprove their existence. More experiments are here needed for a definite answer.

Another body of information on the structure of ^3He impurity states is provided by the specific-heat measurements of Gasparini and coworkers³²⁻³⁴ on mixture films. The data are analyzed in Ref. 33 with a model allowing for several surface states, and values are obtained for the energies and effective masses of the first two states, as functions of ^3He coverage and film thickness; the authors indicate that the energy difference $\Delta\varepsilon$ is better determined than each energy separately. As mentioned in the introduction, thin films are strongly perturbed by the substrate potential, and bulk states are subject to a finite size quantization. However the thickest films considered in Ref. 33 are of more than 40 \AA , so that the substrate potential in the surface region is completely negligible; also, in these thick films, surface states are not expected to be sensitive to the finiteness of the film; hence they are certainly representative of the bulk surface, and this is confirmed by the results of Ref. 18. Now from Fig. 14 of Ref. 33, it appears that for thick films and for a coverage of 0.28–0.29 atomic layer, i.e., 0.18 \AA^{-2} , the energy difference $\Delta\varepsilon$ is in the range 1.7–1.8 K. It is suggested in Ref. 33 that $\Delta\varepsilon$ should tend to an asymptotic value of 2.2 K, equal to the difference between the energy of a ^3He atom dissolved in the bulk and the impurity state energy of -5 K , as determined by Edwards *et al.* However, we do not see any physical effect able to increase $\Delta\varepsilon$ by 0.4–0.5 K, when going from a film of 45 \AA (for which the Nucleopore substrate potential is of the order of a millikelvin at the surface) to the bulk surface. To the contrary, the data are compatible with, and indeed point to the persistence, on the bulk surface, of the mentioned value of 1.7–1.8 K. The present calculations, for the same ^3He coverage of 0.28–0.29 atomic layer, predicts a value $\Delta\varepsilon = 1.45 \text{ K}$. The discrepancy may not be really significant, in view of the fact that the more elaborate theory of Ref. 19 gives, for $N_s = 0$, a value of $\Delta\varepsilon$ larger than the present one by 0.25 K. If the present interpretation is correct, then the heat capacity measurements of Refs. 32–34 provide the first evidence, not fully recognized at the time, that the ^4He bulk surface accommodates at least two ^3He impurity states.

5. CONCLUSIONS

In the present paper, we have studied, using a self-consistent mean-field approach, the structure of the surface states of ^3He atoms on liquid ^4He at

zero temperature. We have found that three types of surface states are accessible to the ${}^3\text{He}$ impurities; the corresponding wave functions differ in the direction perpendicular to the surface, having no node, one node and two nodes. In the limit $N_s \rightarrow 0$, the energies and effective masses of the two lowest states of each kind are respectively $(-5.44 \text{ K}, 1.29m_3)$, $(-3.61 \text{ K}, 1.60m_3)$. The third state has an energy close to that of a ${}^3\text{He}$ atom dissolved in the bulk and an effective mass of $2.23m_3$. When N_s increases, the lowest energy is pushed up as the average field becomes less attractive, but the enlarging of the well is such that the energy of the first excited state remains roughly constant while that of the second excited state decreases slightly.

For ${}^3\text{He}$ coverage up to $N_s \approx 0.035 \text{ \AA}^{-2}$ (i.e., half a monolayer of ${}^3\text{He}$ atoms) the first continuum only is occupied. We find that, to a good accuracy, the single-particle spectrum follows the law of a two-dimensional Fermi gas model, the ground-state energy depending linearly on N_s . We also find that the effective mass for each type of state increases with N_s ; in the range $0 \leq N_s \leq 0.02 \text{ \AA}^{-2}$ the effective mass associated with the first continuum increases from $M_0/m_3 = 1.29$ to 1.45, which covers the range of values extracted from experiment using a model which does not allow for such a dependence of M_0 on N_s .

For values of $N_s \geq 0.035 \text{ \AA}^{-2}$, the second type of continuum states (which have one node in the direction perpendicular to the surface) starts being occupied. Two effects result from the second continuum (i) the surface tension shows a kink as a function of ${}^3\text{He}$ coverage N_s and, more clearly, (ii) the surface specific heat shows a discontinuity due to the fact that the single particle density of states increases by a factor of almost two. A second step is predicted to occur when the continuum built on the second excited state starts being occupied, i.e., for ~ 1.3 atomic layers. The existence of several surface states implies that the ${}^4\text{He}$ surface can support more ${}^3\text{He}$ atoms than usually assumed before they start penetrating into the bulk liquid by occupying bulk states. By extrapolating our results, we find that N_s^{max} is of the order of 1.5 to two atomic layers, i.e. at least half a monolayer more than quoted in Ref. 5.

The physical picture emerging from the present work provides an explanation for the rise in C_V/T observed by Edwards and coworkers³¹ from surface-tension measurements. It suggests also a new interpretation to the heat capacity measurements in *thick* mixture films by Gasparini and coworkers.³²⁻³⁴ The fact that these data were not considered at the time as an indication that the bulk surface could accommodate at least *two* ${}^3\text{He}$ impurity states may simply be due to the lack of a theoretical model predicting such a structure. This structure of states should also produce steps in the magnetization of the system, as observed in thin films by Hallock and coworkers.³⁰

A direct experimental confirmation of the present analysis would also provide indirect indication on the width of the surface profile of pure liquid ${}^4\text{He}$; as indicated in the introduction, the presence of several surface states is linked to a value of the surface width of the order of 6 to 7 Å.

APPENDIX

We derive here Eq. (22). Let us write explicitly the density functional of Eqs. (6a and b). The function $U(\rho_3, \rho_4)$ appearing in Eq. (6b) reads as

$$U(\rho_3, \rho_4) = \frac{1}{2}b_3\rho_3^2 + \frac{1}{2}c_3\rho_3^2(\rho_3 + \rho_4)^{\gamma_3} + \frac{1}{2}\tilde{c}_3\rho_3^{2+\gamma_3} + b_{34}\rho_3\rho_4 + c_{34}\rho_3\rho_4(\rho_3 + \rho_4)^{\gamma_{34}} \\ + \frac{1}{2}b_4\rho_4^2 + \frac{1}{2}c_4\rho_4^2(\rho_3 + \rho_4)^{\gamma_4} \quad (\text{A.1})$$

The mean-field equations are given in 10a and b. We can multiply Eq. (10a) by $\phi_3^{i,k}$, sum over i and integrate over k , multiply Eq. (10b) by ρ_4 , add them together and integrate over all space to obtain

$$\int d^3r \left\{ \frac{\hbar^2}{2m_3^*} \tau_3 + \tau_3 \left[\rho_3 \frac{\partial}{\partial \rho_3} + \rho_4 \frac{\partial}{\partial \rho_4} \right] \left(\frac{\hbar^2}{2m_3^*} \right) \right. \\ + b_3\rho_3^2 + \frac{2+\gamma_3}{2} c_3\rho_3^2(\rho_3 + \rho_4)^{\gamma_3} + \frac{2+\gamma_3}{2} \tilde{c}_3\rho_3^{2+\gamma_3} + 2d_3|\nabla\rho_3|^2 \\ + 2b_{34}\rho_3\rho_4 + 2d_{34}\nabla\rho_3\nabla\rho_4 + (2+\gamma_{34})c_{34}\rho_3\rho_4(\rho_3 + \rho_4)^{\gamma_{34}} \\ \left. + \frac{\hbar^2}{8m_4} \frac{|\nabla\rho_4|^2}{\rho_4} + b_4\rho_4^2 + \frac{2+\gamma_4}{2} c_4\rho_4^2(\rho_3 + \rho_4)^{\gamma_4} + 2d_4|\nabla\rho_4|^2 \right\} \\ = \mu_4 \int \rho_4 d^3r + \sum_i \int_0^{k_{f_i}} \frac{k dk}{\pi} \varepsilon_{i,k} \quad (\text{A.2})$$

By comparing with Eq. (A.1) and Eq. (17), one gets

$$\sigma = \sum_i \int_0^{k_{f_i}} \frac{k dk}{\pi} \varepsilon_{i,k} - \mu_3 N_s - \int dz \left\{ \tau_3 \left[\rho_3 \frac{\partial}{\partial \rho_3} + \rho_4 \frac{\partial}{\partial \rho_4} \right] \left(\frac{\hbar^2}{2m_3^*} \right) \right. \\ + \frac{1}{2} b_3\rho_3^2 + \frac{c_3}{2} \rho_3^2(1+\gamma_3)(\rho_3 + \rho_4)^{\gamma_3} + \frac{\tilde{c}_3}{2} (1+\gamma_3)\rho_3^{2+\gamma_3} + d_3\rho_3'^2 \\ + b_{34}\rho_3\rho_4 + c_{34}(1+\gamma_{34})\rho_3\rho_4(\rho_3 + \rho_4)^{\gamma_{34}} + d_{34}\rho_3\rho_4' \\ \left. + \frac{1}{2} b_4\rho_4^2 + \frac{c_4}{2} (1+\gamma_4)\rho_4^2(\rho_3 + \rho_4)^{\gamma_4} + d_4\rho_4'^2 \right\} \quad (\text{A.3})$$

The first two terms in the right-hand side correspond to the ideal 2-DFG model, as can be easily checked using Eq. (19a). For low coverage, one considers only the lowest states, with energy $\epsilon_{0,k}$; thus

$$\begin{aligned} \int_0^{k_{f_0}} \frac{k dk}{\pi} \epsilon_{0,k} - \mu_3 N_s &\approx \int_0^{k_{f_0}} \frac{k dk}{\pi} \left(\epsilon_{0,0} + \frac{\hbar^2}{2m_0^*} k^2 \right) - \left(\epsilon_{0,0} + \frac{\hbar^2 k_F^2}{2m_0^*} \right) \frac{k_F^2}{2\pi} \\ &\approx -\pi \frac{\hbar^2}{2m_0^*} N_s^2 \end{aligned} \quad (\text{A.4})$$

Next, by considering the case $N_s = 0$, one recognizes in Eq. (A.3) the surface tension σ_4 of pure liquid ⁴He. Since we know from Eq. (21) that $\sigma - \sigma_4$ is a quadratic function of N_s for low N_s , one can write

$$\sigma \approx \sigma_4 - \pi \frac{\hbar^2}{2m_0^*} N_s^2 - (\Sigma_{33} + \Sigma_{34} + \Sigma_{44}) N_s^2 \quad (\text{A.5})$$

with obvious notations. In the work of Edwards *et al.*,^{4,5} the different components of the interaction contribution are represented by a single effective surface ³He-³He interaction coefficient written as V_0^s , which appears also in Eq. (1). It is formally equivalent to the term in b_3 of the present functional.

The different coefficients Σ_{33} , Σ_{34} , and Σ_{44} are numerically calculated in the following way. Having solved the mean-field equations for a given coverage, we perform a scaling on the equilibrium densities ρ_3 and ρ_4 in the form

$$\begin{aligned} \rho_3(z) &\rightarrow \alpha_3 \rho_3(z) \\ \rho_4(z) &\rightarrow \rho_4^0(z) + \alpha_4 (\rho_4(z) - \rho_4^0(z)) \end{aligned}$$

where $\rho_4^0(z)$ represents the surface profile of pure ⁴He. We then introduce these scaled densities into Eq. (17). This produces a function $\sigma(\alpha_3, \alpha_4)$ which is a quadratic form in α_3 and α_4

$$\sigma(\alpha_3, \alpha_4) \approx \sigma_4 - \left(\Sigma_{33} + \pi \frac{\hbar^2}{2m_0^*} \right) N_s^2 \alpha_3^2 - \Sigma_{34} \alpha_3 \alpha_4 N_s^2 - \Sigma_{44} \alpha_4^2 N_s^2 \quad (\text{A.6})$$

when the first continuum only is occupied, and

$$\begin{aligned} \sigma(\alpha_3, \alpha_4) &\approx \sigma_4 - \left[\Sigma_{33} + \pi \frac{\hbar^2}{2m_0^*} \left(\frac{k_{f_0}^2}{2\pi} \right)^2 + \pi \frac{\hbar^2}{2m_1^*} \left(\frac{k_{f_1}^2}{2\pi} \right)^2 \right] \alpha_3^2 \\ &\quad - \Sigma_{34} \alpha_3 \alpha_4 N_s^2 - \Sigma_{44} \alpha_4^2 N_s^2 \end{aligned} \quad (\text{A.7})$$

when the second continuum also is occupied. The Σ 's are determined from Eqs. (A.6) and (A.7) through a quadratic fit of the function $\sigma(\alpha_3, \alpha_4)$. We

find that the sum $\Sigma = \Sigma_{33} + \Sigma_{34} + \Sigma_{44}$ is always positive and contributes to decrease σ . This is in agreement with the result of Ref. (4). One cannot hope to extract these three coefficients from experiment; rather we want to point out here that, besides the contribution due to the ${}^3\text{He}$ - ${}^3\text{He}$ effective interaction, other effects of the same order of magnitude contribute to Σ . The sign of Σ results of a balance between the negative rearrangement terms (Σ_{33} and Σ_{44}) and the positive interaction term (Σ_{34}).

The method exposed above is strictly valid only for weak coverages. However, formulas (A.6) and (A.7) give a reasonable fit to the total surface tension up to $N_s \approx 0.06 \text{ \AA}^{-2}$. In our approach the Σ 's depend on N_s (whereas in Ref. (4) V_0^s does not). The total sum Σ (which is to be compared to $V_0^s/4$) varies from 10.2 K\AA^2 to about 1 K\AA^2 for $N_s = 0.067 \text{ \AA}^{-2}$.

ACKNOWLEDGEMENT

It is a pleasure to acknowledge useful discussions with F. Dalfovo. We also would like to thank warmly D. O. Edwards for his interest in this work and for communicating to us the unpublished results by D. B. Crum, D. O. Edwards, and R. Sarwinski contained in D. B. Crum's thesis.

REFERENCES

1. A. F. Andreev, *Zh. Eksp. Teor. Fiz.* **50**, 1415 (1966) [*Sov. Phys.-JETP* **23**, 939 (1966)].
2. H. M. Guo, D. O. Edwards, R. E. Sarwinski, and J. T. Tough, *Phys. Rev. B* **20**, 4518 (1975).
3. D. Crum, D. O. Edwards, and R. E. Sarwinski, *Low Temperature Physics LT-14*, M. Krusius and M. Vuorio, eds. (North-Holland, Amsterdam, 1975), Vol. 1, p. 423.
4. D. O. Edwards, S. Y. Shen, J. R. Eckardt, P. P. Fatouros, and F. M. Gasparini, *Phys. Rev. B* **12**, 892 (1975).
5. D. O. Edwards and W. F. Saam in *Progress in Low Temperature Physics*, D. F. Brewer, ed. (North-Holland, Amsterdam, 1978), Vol. VII A, p. 283.
6. G. Deville, *J. Low Temp. Phys.* **72**, 135 (1988).
7. A. F. Andreev and D. A. Kompaneets, *Zh. Eksp. Teor. Fiz.* **61**, 2459 [*Sov. Phys.-JETP* **34**, 1316 (1972)].
8. J. Lekner, *Philos. Mag.* **22**, 669 (1970).
9. W. F. Saam, *Phys. Rev. A* **4**, 1278 (1971).
10. Y. M. Shih and C. W. Woo, *Phys. Rev. Lett.* **30**, 478 (1973).
11. C. C. Chang and M. Cohen, *Phys. Rev. A* **8**, 3131 (1973).
12. D. S. Sherrill and D. O. Edwards, *Phys. Rev. B* **31**, 1338 (1985).
13. F. Dalfovo and S. Stringari, *Physica Scripta* **38**, 204 (1988).
14. F. Dalfovo, *Z. Phys. D* **14**, 263 (1989).
15. S. Stringari and J. Treiner, *Phys. Rev. B* **36**, 8369 (1987).
16. V. R. Pandharipande, J. G. Zabolitzky, S. C. Pieper, R. B. Wiringa, and U. Helmbrecht, *Phys. Rev. Lett.* **50**, 1676 (1983).
17. J. Dupont-Roc, M. Himbert, N. Pavloff, and J. Treiner, *J. Low Temp. Phys.* **81**, 31 (1990).
18. N. Pavloff and J. Treiner, Orsay preprint IPNO/Th 90-52, July, 1990, submitted to *J. Low Temp. Phys.*
19. R. H. Anderson and M. Miller, *Phys. Rev. B* **40**, 2109 (1989).
20. D. O. Edwards and P. P. Fatouros, *Phys. Rev. B* **17**, 2147 (1978).

21. N. Pavloff and J. Treiner, in preparation.
22. E. Krotscheck, *Phys. Rev. B* **32**, 5713 (1985).
23. E. Krotscheck, M. Saarela, and J. L. Epstein, *Phys. Rev. B* **38**, 111 (1988).
24. S. Stringari and J. Treiner, *J. Chem. Phys.* **87**, 5021 (1987).
25. F. Dalfovo and S. Stringari, *Phys. Lett. A* **112**, 171 (1985).
26. F. Dalfovo, Ph.D. Thesis, Trento (1989), unpublished.
27. T. H. R. Skyrme, *Philos. Mag.* **1**, 1043 (1956); T. H. R. Skyrme, *Nucl. Phys.* **9**, 615 (1959); M. Beiner, H. Flocard, N. V. Giai, and P. Quentin, *Nucl. Phys. A* **238**, 29 (1975).
28. *Handbook of Mathematical Functions*, M. Abramowitz and I. A. Stegun, eds. (Dover, N.Y., 1972).
29. R. A. Guyer, K. R. McCall, and D. T. Sprague, *Phys. Rev. B* **40**, 7417 (1989).
30. R. H. Higley, D. T. Sprague, and R. B. Hallock, *Phys. Rev. Lett.* **63**, 2570 (1989) and references therein.
31. D. B. Crum, Ph.D. Thesis, Ohio State University (1973), unpublished.
32. J. Di Pirro and F. M. Gasparini, *Phys. Rev. Lett.* **44**, 269 (1980).
33. B. K. Bhattacharyya, M. J. Di Pirro, and F. Gasparini, *Phys. Rev. B* **30**, 5092 (1984).
34. F. M. Gasparini, B. Bhattacharyya, and M. J. Di Pirro, *Phys. Rev. B* **29**, 4921 (1984).